AD-A131 408 ULTRASOUND TOMOGRAPHY BY GALERKIN OR MOMENT METHODS(U) 1/1
UTAH UNIV SALT LAKE CITY DEPT OF MATHEMATICS
S A JOHNSON ET AL. 05 MAY 83 ARO-19297.2-MA
UNCLASSIFIED DAAG29-83-K-0012 F/G 6/2 NL

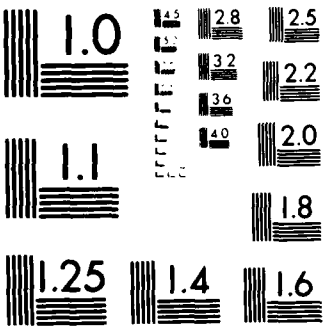

ULTRASOUND TOMOGRAPHY BY GALERKIN OR MOMENT METHODS

Steven A. Johnson
Department of Bioengineering
Department of Electrical Engineering

and

Frank Stenger*
Department of Mathematics
University of Utah
Salt Lake City, Utah 84112

*Supported by U. S. Army Research Contract Number DAAG-29-83-K-0012.

83 08 15 025

May 5, 1983

INTRODUCTION

Ultrasound B-scan imaging is now a well established and valuable clinical tool. Inprovements in transducer arrays and microprocessor controls have lead to the development of real time linear and sector scanners which produce images of remarkable clarity and resolution compared with B-scanners of only a few years ago. Further improvements in B-scan images are predicted to occur as larger transducers apertures and improved dynamic focusing methods are employed. The use of Doppler ultrasound alone or in combination with real time B-scan imaging is expected to increase in importance as the clinical significance of high resolution Doppler images is appreciated.

During the past decade X-ray C.T. (computed tomography) and recently NMR imaging have made remarkable contributions to the field of diagnostic imaging. X-ray (C.T.) and NMR images not only provide resolution of about 1 mm but also can be calibrated by absolute reference standards. The resulting quantitative images have proven to have valuable diagnostic value because of the greater ability thus provided to distinguish healthy and diseased tissue by their image values.

It is natural to ask if the successful B-scanner technology could be improved further by incorporating quantitative tissue characterization features. Such tissue characterization features, based on back scatter, are now being investigated for inclusion on clinical B-scanners, but the tissue characterization they provide is based on structural and statistical properties of tissues and not absolute tissue properties. The statistical properties of tissues, e.g., the spatial Fourier transform, are often correlated with the state of health or disease and are therefore valuable but they are not easy to measure quantitatively with back scatter techniques unless special precautions are taken to model or compensate for angular dependence. These back scatter statistical properties are dependent on the gradient of the density of the tissues and thus the constant of integration

has been lost [1]. Thus we have partially answered our question. We have noted that some quantitative information about tissue properties can be obtained from B-scans but not the absolute mechanical properties of tissue. It is then appropriate to ask if ultrasound can in principle provide additional tissue properties. The answer is yes if the scattering into many angles is used. We next describe how such scattering has been investigated for imaging applications.

During the past decade many investigators have attempted to develop an ultrasound tomography which could provide resolution and absolute tissue characterization analogous to x-ray C.T. The first ultrasound C.T. systems appeared at about the same time that NMR imaging was demonstrated and shortly after x-ray C.T. was announced [2,3]. The development of ultrasound C.T. has not shown the rapid development into a clinical tool as have the other modes. The rapid development of NMR imaging has been surprising even to many closely associated with medical imaging. The reasons why ultrasound imaging has not followed the same pace is now becoming more clear.

Ultrasound C.T. has not made the rapid progress of x-ray C.T. or NMR imaging for several reasons: (1) the theory for x-ray C.T. or NMR imaging is much simpler than that of ultrasound C.T.. (2) neither x-ray or NMR imaging are subject to diffraction and refraction effects, but these two effects dominate the ultrasound signal detection process. (3) x-ray detector arrays and NMR detectors are relatively simple to design and build compared to ultrasound detector arrays. This chapter will address suggestions for improving the resolution and quantitative imaging of ultrasound C.T. by addressing the theory for ultrasound C.T. and treating refraction and diffraction effects.

Initial attempts to develop ultrasound C.T. greatly simplified the problem by treating the propagation of ultrasound as if the acoustic energy followed straight line rays like x-rays. As a consequence, refraction and diffraction effects limited resolution to about 10 to 20 wavelengths. Correcting for refraction

of the ray paths did not help because resolution is determined mostly by diffraction effects. As the diffraction problem became better understood several investigators suggested including diffraction and refraction in the ultrasound imaging formulations by borrowing Wolf's clever perturbation theory, inverse Born, scattering algorithm from optical holography theory [4,5]. Much effort has been expended in developing this approach with the greatest success coming from replacing the Born approximation with the more accurate Rytov approximations. Although this work has brought fresh and important insight to the quest, there are several serious defects in these Rytov or Born perturbation methods [6]: (1) these methods must assume unrealistically low absorption. (2) the refraction is only treated approximately, e.g., the far field of a simple lens is not given correctly by either the Born or Rytov approximate methods. (3) the inclusion of density scattering has been solved but still depends on attenuation being treated correctly.

The use of an attenuating bath has been suggested to allow imaging of human tissue at higher frequencies, e.g., 1 to 3 mhz. A new algorithm to allow better treatment of refraction effects for ultrasound C.T. has been proposed [7]. Such approaches may help, yet the fact remains that the perturbation methods are not exact except in the limit of vanishingly small perturbations. Therefore, an ultrasound imaging method based upon a more exact treatment of the wave equation would have the capability of imaging objects with larger attenuation and larger variations in refractive index and density. Such a method would also have the desirable feature of acting as a standard of comparison.

We are aware of two methods which do not depend on the object producing only small perturbations to the total field. The first method is based upon extrapolating the scattered data to zero wavelength. This method looks promising for medical imaging and has potential for wider development and use if its sensitivity to noise can be reduced [8,9].

The second method is less sensitive to noise and provides "exact" inverse scattering solutions (by exact we mean the equation or theoretical model used for imaging contains no unrealistic or major approximations). The second method although "exact" in the above sense is nevertheless iterative in nature and may probably require a later generation of computers for cost effective implementation. Nevertheless, the method is of academic and laboratory significance and may serve as the starting point for further improvements in ultrasonic imaging; a description follows.

ULTRASONIC IMAGING BY SOLUTION OF THE INVERSE SCATTERING PROBLEM

The ultrasound imaging problem in its most general and complete form is equivalent to solving the so-called inverse scattering problem. The inverse scattering problem may be defined as finding the spatial distribution γ of material properties so that the wave equation scattered field solutions $f^{(s)}$ for any incident field $f^{(i)}$ matches the given scattered field. The solution to the direct scattering problem is defined to be the solution $f^{(s)}(x)$ to a wave equation at some point x for γ given. Thus, the solution γ to the inverse scattering problem is that γ for which the solution to the direct scattering problem matches given scattered field values. In the usual ultrasound imaging environment only the scattered fields on a detector are given by measurement, but the scattered fields within the object are not known. If the fields were known within the object then the solution to the inverse scattering problem could be obtained by a linear operation. Since both the internal field and material property are unknown, the solution to the inverse scattering problem also requires, at least implicitly, the solution to the direct scattering problem.

Because of the past difficulty of solving the inverse scattering problem, approximate solutions have been developed. One of the most widely known approximation methods is based upon using first order perturbation theory to linearize the procedure for solving the wave equation as a function of γ. This approach leads to the derivation of the well known Born and Rytov approximations [5]. For the Born

approximation, equations for the perturbation in the acoustic pressure field p and perturbation in material properties γ are given by the equations

$$p = p_0 + p_1 \tag{1}$$

$$\gamma = \gamma_0 + \gamma_1 \tag{2}$$

where p is the total field when $\gamma = \gamma_0 + \gamma_1$ and p_2 is the field when $\gamma = \gamma_0$ where γ_0 is a constant and is the material property of the homogeneous background [5]. The Rytov approximation is obtained by the transformations

$$p = \exp(W) \tag{3}$$

$$W = W_0 + W_1 \tag{4}$$

where W_0 is the logarithm of the incident field when $\gamma_1 = 0$, where W is the logarithm of the total field when $\gamma = \gamma_0 + \gamma_1$ and where W_1 is the pertubation in W caused by the perturbation γ_1 in γ.

For medical applications, the assumption that γ_1, p_1, and W are small with respect to γ_0, p_0, and W_0, respectively, may in many cases be erroneous because of refraction and attenuation. This may be seen by inspection of the Helmholtz wave equation

$$\nabla^2 p(\underline{x}) + \frac{\omega^2}{[c(\underline{x})]^2} p(\underline{x}) = 0 \quad . \tag{5}$$

The speed of sound $c(\underline{x})$ may be considered to be complex and we could write $c(\underline{x}) = c_R(x) + ic_I(x)$. However it is more convenient to first expand $[c(\underline{x})]^{-2}$ by

equation (2) before examining the real and imaginary parts. By adding $k_0^2 F(\underline{x})p(\underline{x}) = \omega^2(c_0^{-2} - [c(\underline{x})]^{-2})p(\underline{x})$ to both sides of equation (5) we obtain

$$\nabla^2 p(\underline{x}) + k_0^2[1 - F(\underline{x})]p(x) = 0 \tag{6}$$

where $k_0^2 = \omega^2/c_0^2$ is the background wave number squared. Thus by inspection of equation (2) we see that $\gamma_0 = k_0^2$ and $\gamma_1 = F(\underline{x})k_0^2$. We now consider two examples which illustrate the effect of $F(\underline{x})$ on the relative sizes of p_0 and p_1.

The first example is that of a simple lens. It is clear that a small value of $F(\underline{x})$, say five or ten percent, distributed in a lens shaped region can focus an incident plane wave to a local zone where the total field p may be many times larger than the unperturbed field p_0. Thus, the scattered or perturbed field p_1 can not be small in comparison to p_0. The second example is that of a plane wave normally incident upon a block of homogeneous material with a small but finite loss corresponding to the imaginary part of $F(\underline{x})$. It is easily shown that even though the imaginary part of $F(\underline{x})$ is small the line integral of the linear acoustical attenuation coefficient can reduce the amplitude of the internal field to a small fraction of the incident field in only 10 cm. of travel. Soft tissue has an attenuation of only about 1 db cm^{-1} MHz^{-1}. For an average speed of sound of 1500 m. sec^{-1} and at 1 MHz, 1 $dbMHz^{-1}$ cm^{-1} corresponds to a ratio of imaginary to real part of the wave number of about 0.005. Nevertheless, at 1 MHz at a depth of 10 cm in the block the field is down 10 db relative to the field at the surface, that is, the pressure is reduced by 68 percent.

These examples illustrate the need for caution when applying the Born or Rytov theory. The situation can be improved if the background fluid is tailored to have a real and imaginary speed of sound equal to the mean respectively of the real and imaginary parts of the speed of sound for the object in the background fluid. A method for obtaining an inverse scattering solution to the exact Helmholtz

wave equation or which does not require actual field to be nearly equal to the incident field with no object present, would avoid difficulties illustrated by the two examples above. We next review the background of a method for obtaining a direct solution to the exact Helmholtz wave equation which we will use to develop a robust inverse scattering solution to the exact Helmholtz wave equation.

Methods for solving the direct scattering problem by the method of moments, of which the Galerkin method is a special case, are presented in the book by Harrington [10] and the paper by Richmond [11]. Recently the method of Richmond was adapted independently by Hagmann [12] and by Yoon et al [13] to solve the inverse scattering problem for the case of a single source. They found that the inverse scattering problem for a single source is an ill-posed problem and therefore very small amounts of noise in the data caused a large amount of noise in the solution for γ . As the number of points in the image domain grows, the condition number of the matrices to be inverted by the single source method grows rapidly and the solution becomes unstable and inaccurate. The stability of the solution also decreased as the detector to object distance was increased.

The ill-posed nature of the inverse scattering solution may be largely removed by solving a system of nonlinear equations resulting from using multiple sources [14]. The multiple source solution has demonstrated good tolerance to additive noise in the scattering date and is not sensitive to the position of the detection for over-determined cases.

FORMULATION OF EQUATIONS WHICH MAY BE SOLVED FOR DIRECT AND INVERSE SCATTERING SOLUTIONS

We now introduce an improved wave equation containing equation (6) as a special case and introduce an equivalent integral equation. We then transform the integral equation into a set of multivariate quadratic equations. The solution to these quadratic equations lends to the direct scattering solution and the inverse scattering solution.

The wave equation for a body immersed in a homogeneous fluid is given by [1]

$$(7) \qquad \nabla^2 f_\emptyset(\underline{x}) + k_0^2 f_\emptyset(\underline{x}) = -k_0^2 \gamma_\kappa(\underline{x}) f_\emptyset(\underline{x}) - \nabla\cdot[\gamma_\rho(\underline{x})\nabla f_\emptyset(x)]$$

where $f_\emptyset(\underline{x})$ is a scalar field such as acoustic pressure for a source at position $\emptyset$, $k_0 = \omega/c_0$, ω = angular frequency of incident field, c_0 is constant speed of sound in a homogeneous background fluid, $\gamma_\kappa = (\kappa - \kappa_0)/\kappa_0$ and $\gamma_\rho = (\rho - \rho_0)/\rho_0$ are the fractional change in compressibility κ and density ρ , respectively outside the body in the fluid background. A useful integral equation which is equivalent to (7) and includes the boundary conditions is [1]

$$(8) \quad f_\emptyset^{(s)}(\underline{x}) \triangleq f_\emptyset(\underline{x}) - f^{(i)}(\underline{x}) = \int [k_0^2 \gamma_\kappa(\underline{x}') f_\emptyset(\underline{x}') g(\underline{x}';\underline{x}) + \int \gamma_\rho \nabla' f_\emptyset(\underline{x}')\cdot\nabla' g(\underline{x}';\underline{x})] d^Q\underline{x}'$$

where $\underline{x} = (x_1,\ldots,x_Q)$, $\underline{x}' = (x_1',\ldots,x_Q)$ are spatial coordinates in a space of dimension $Q \leq 3$, $f_\emptyset^{(s)}(\underline{x})$ is the scattered field $f_\emptyset(\underline{x}) - f_\emptyset^{(i)}(\underline{x})$, $f_\emptyset^{(i)}(\underline{x})$ is the field $f_\emptyset(\underline{x})$ for no object present; i.e., for $\gamma_\kappa = \gamma_\rho = 0$, and where $g(\underline{x}';\underline{x})$ is a Green's function. For two-dimensional problems $g(\underline{x}';x) = H_0^{(2)}(k_0|\underline{x}-\underline{x}'|)$ where $H_0^{(2)}(\cdot)$ is the first order Hankel function of the second kind. For three-dimensional problems $g(\underline{x}';\underline{x}) = (4\pi|\underline{x}-\underline{x}'|)^{-1}\exp(ik_0|\underline{x}-\underline{x}'|)$, and where $|\cdot|$ means absolute value.

We now expand the fields $f_\emptyset, f_\emptyset^{(i)}$, and $f_\emptyset^{(s)}$ and factors containing the material properties using an accurate basis set $\{\psi_i(\underline{x})\}$. Let

$$(9,10) \qquad f_\emptyset(\underline{x}) = \sum_{i=1}^{N} a_{\emptyset i}\,\psi_i(\underline{x}) \quad , \quad f_\emptyset^{(i)}(\underline{x}) = \sum_{i=1}^{N} b_{\emptyset i}\,\psi_i(\underline{x})$$

$$(11,12) \qquad f_{\emptyset}^{(s)}(\underline{x}) = \sum_{i=1}^{N} d_{\emptyset i}\, \psi_i(\underline{x}) \quad , \quad k_0^2\, \gamma_\kappa(\underline{x}')f_{\emptyset}(\underline{x}) = \sum_{i=1}^{N} c_{\emptyset i}\, \psi_i(\underline{x}')$$

$$(13) \qquad \gamma_\rho(\underline{x}')\nabla f_{\emptyset}(\underline{x}') = \sum_{i=1}^{N} \sum_{q=1}^{Q} A_{q\emptyset i}\, \psi_i(\underline{x}')\hat{e}_q \quad ,$$

where N is the number of basis functions and Q is the dimension of the space and corresponding Greens function, and where $\hat{e}_q$ is a unit vector along coordinate q. Upon substitution of (13) into (8) we obtain upon interchaning integration and summation,

$$(14) \qquad \sum_{i=1}^{N} (a_{\emptyset i} - b_{\emptyset i})\psi_i(\underline{x}) = \sum_{j=1}^{N} c_{\emptyset j}\, g_j(\underline{x}) + \sum_{j=1}^{N} \sum_{q=1}^{Q} A_{q\emptyset j}\, G_{qj}(\underline{x})$$

where

$$(15,16) \qquad g_j(\underline{x}) = \int g(\underline{x}';\underline{x})\psi_j(\underline{x}')d^Q\underline{x}' \quad , \quad G_{qj}(\underline{x}) = \int \frac{\partial g}{\partial x_q}\, \psi_j\, d^Q\underline{x}' \quad .$$

Using the "expansion method" equation (14) could be developed into a system of algebraic equations describing the scattering by evaluating (14) at a set of grid points $\{\underline{x}_j\}$. Alternately, by taking the inner product of (14) with all members of a weighting or testing set of basis functions $\{W_i(\underline{x})\}$ a system of N algebraic equations may be generated by the "method of moments" [10]. If $W_i(x) \equiv \psi_i(x)$ for all i and $\{\psi_i\}$ are independent then the procedure becomes the classical "Galerkin method" [10]. If $W_i(x) \equiv \delta(\underline{x}-\underline{x}_i)$ the method of moments becomes the expansion method. The choice of the expansion basis functions $\{\psi_i(\underline{x})\}$ and the testing functions $\{W_i(\underline{x})\}$ is problem dependent and often significantly effects the accuracy of solution and the number of expansion basis functions needed to obtain a solution [10]. The sinc basis functions have many properties which make them especially attractive for applications using the method of moments and in the remaining sections we will use only basis sets based on the sinc functions.

ALGEBRAIC SCATTERING EQUATIONS DERIVED USING SINC BASIS FUNCTIONS

The sinc functions are attractive as a basis set because when properly formulated the basis set is complete, orthogonal and retains some local or regional properties (by local or regional we mean that each coefficient of the basis expansion are related to the values of the function to be expanded in a unique local region and this property often aids in incorporating measurements or boundary conditions) for representing spatially band limited functions.

In one-dimensions a function $f(x)$ may be expanded in a basis set consisting of sinc functions shifted in integral multiples of step size h as follows

$$f(x) \approx C(f,h) \triangleq \sum_{\ell=-\infty}^{\infty} f(\ell h) S(\ell,h)(x) \tag{17}$$

where the shifted sinc functions are given by

$$S(\ell,h)(x) \triangleq \frac{\sin[(\pi/h)(x-\ell h)]}{(\pi/h)(x-\ell h)} \quad . \tag{18}$$

If $f(x)$ is band limited to contain no Fourier components greater than π/h then $f(x) = C(f,h)$. The orthogonality of $\{S(\ell,h)(x)\}$ is expressed by

$$\int_{-\infty}^{\infty} C(f,h)(t) S(\ell,h)(t)\,dt = h\, f(\ell h) \quad . \tag{19}$$

The nth derivative of function $C(f,h)$ has a sinc expansion given by

$$\left(\frac{d}{dx}\right)^n C(f,h)(x) = h^{-n} \sum_{j=-\infty}^{\infty} \{\sum_{\ell} \delta_{\ell j}^{(n)} f(\ell h)\} S(j,h)(x) \tag{20}$$

$$\delta_{\ell j}^{(n)} = \frac{d^n}{dx^n} S(\ell,1)(x)\Big|_{x=j} \quad . \tag{21}$$

In particular

$$\delta^{(1)}_{\ell j} = \begin{cases} 0 & , \quad \ell = j \\ (-1)^{j-\ell}\,(j-\ell)^{-1} & , \quad \ell \neq j \end{cases} . \tag{22}$$

The cardinal function $C(f,h)$ may be integrated by use of the following formula

$$\int_{-\infty}^{\infty} C(f,h)(t)\,dt = h \sum_{\ell=-\infty}^{\infty} f(\ell h) . \tag{23}$$

These and other useful properties of the sinc function for solving integral equations and for other applications are given by Stenger [15].

We take products of Q sinc functions to form basis sets for problems in Q dimensions. We illustrate this for two dimensions by setting

$$\psi_{i(m,n)}(\underline{x}) = S(m,h)(x_1)S(n,h)(x_2) \tag{24}$$

to obtain

$$f_{\emptyset}(x_1,x_2) = \sum_m \sum_n f_{\emptyset}(mh,nh)S(m,h)(x_1)S(n,h)(x_2) . \tag{25}$$

Here $i = i(m,n)$ means i is an index which indexes point (m,n) in a finite two dimensional array of grid points. Thus by (9-12), (24,25) and by property (17) we obtain relationships for the coefficients $a_{\emptyset i}$, $b_{\emptyset i}$, $c_{\emptyset i}$ as follows

$$a_{\emptyset i(m,n)} = f_{\emptyset}(mh,nh) \quad , \quad b_{\emptyset i(m,n)} = f^{(1)}_{\emptyset}(mh,nh) \tag{26,27}$$

$$d_{\emptyset i(m,n)} = f^{(s)}_{\emptyset}(mh,nh) \quad , \quad c_{\emptyset i(m,n)} = k_0^2\,\gamma_{\kappa}(mh,nh)f_{\emptyset}(mh,nh) . \tag{28,29}$$

The relationship between $A_{q\emptyset j}$, γ_ρ , and $f_\emptyset$ is obtained by noting that $\gamma_\rho \nabla' f \cdot \nabla' g = \gamma_\rho(\underline{x}') \sum_q (\partial f/\partial x_q')\ (\partial g/\partial x_q')$. We examine the factor $\gamma_\rho(\underline{x}')(\partial f/\partial x_q')$ and note that $(\partial f/\partial x_q')$ has a sinc expansion via application of (20,21) to (23). The result is the product of γ_ρ and a sinc expansion of $(\partial f/\partial x_q')$. We next perform a sinc expansion on the product by use of (17). These nested expansions are simplified by noting that $S(\ell,h)(x = rh) = \delta_{\ell r}$ (where $\delta_{\ell r} = 0$ if $\ell \neq r$ and $\delta_{\ell r} = 1$ if $\ell = r$) . Applying these steps for the terms $\gamma_\rho(\partial f/\partial x_1)$ and $\gamma_\rho(\partial f/\partial x_2)$ we obtain on setting $x_1 = x$, $x_2 = y$

$$(30a) \qquad \gamma_\rho(x,y)\,\frac{\partial f_\emptyset(x,y)}{\partial x} = h^{-1} \sum_m \sum_n \gamma_\rho(mh,nh) \sum_\ell [\delta^{(1)}_{\ell m}\ f_\emptyset(\ell h,nh)]S(m,h)(x)S(n,h)(y)$$

$$(30b) \qquad \gamma_\rho(x,y)\,\frac{\partial f_\emptyset(x,y)}{\partial y} = h^{-1} \sum_m \sum_n \gamma_\rho(mh,nh) \sum_\ell [\delta^{(1)}_{\ell n}\ f_\emptyset(mh,\ell h)]S(m,h)(x)S(n,h)(y) \ .$$

We now have obtained expressions for $a_{\emptyset i}$, $b_{\emptyset i}$, $c_{\emptyset j}$, $d_{\emptyset j}$ and $A_{q\emptyset j}$ in terms of $f_\emptyset(mh,nh)$, k_0^2 , $\gamma_\kappa(mh,nh)$ and $\gamma_\rho(mh,nh)$ as per (26-29) and (30). These expressions could be substituted into (14) to obtain a set of equations with coefficients $\psi_i(\underline{x})$, $g_j(\underline{x})$ and $G_{gj}(\underline{x})$ to be evaluated. Instead of evaluating the coefficients at all grid points (mh,nh) we use the Galerkin method to expand $g_j(\underline{x})$ and $G_{qj}(\underline{x})$ in terms of $\psi_i(\underline{x})$. Let

$$(31,32) \qquad g_j(\underline{x}) = \sum_i g_{ji}\ \psi_i(\underline{x}) \quad \text{and} \quad G_{qj}(\underline{x}) = \sum_i G_{qji}\ \psi_i(\underline{x})$$

where $\psi_i(\underline{x})$ is given by (24). Thus, by (25) the coefficients g_{ji} and G_{qji} are given by

$$(33,34) \qquad g_{ji} = g_j(\underline{x}_i) \quad \text{and} \quad G_{qji} = G_{qj}(\underline{x}_i) \ .$$

On substitution of (26-29), (30) and (31,32) into (14) we obtain a set of equations involving only

$$f_{\emptyset}(mh,nh)\ ,\ k_0^2\ ,\ \gamma_\kappa(mh,nh)\ ,\ \gamma_\rho(mh,nh)\ ,\ g_{ji}\ ,\ G_{qji}\ ,\ \text{and}\ \ \psi_{i(m,n)}(\underline{x})\ .$$

Thus on factoring, we obtain

$$(35)\qquad \sum_i f_{\emptyset i}^{(s)}\ \psi_i \triangleq \sum_i (f_{\emptyset i} - f_{\emptyset i}^{(i)})\psi_i \;=\; \sum_i \sum_j [k_0^2\ \gamma_\kappa(\underline{x}_j) f_{\emptyset}(\underline{x}_j) g_{ji} + \sum_q A_{q\emptyset j}\ G_{qji}]\psi_i$$

where the sum over $A_{q\emptyset j}$ represents the complete expressions for (30). According to the Galerkin method we may eliminate the factor ψ_i by taking the inner product of (35) with ψ_j. Let us introduce the natural notation $f_{\emptyset}(mh,nh) \triangleq f_{\emptyset i(m,n)} \triangleq f_{\emptyset(m,n)}$, $\gamma_\kappa(mh,nh) \triangleq \gamma_{\kappa i(m,n)} \triangleq \gamma_{\kappa(m,n)}$, $\gamma_\rho(mh,nh) \triangleq \gamma_{\rho i(m,n)} \triangleq \gamma_{\rho(m,n)}$, $g_{j(r,t)i(m,n)} \triangleq g_{ji} \triangleq g_{(r,t)(m,n)}$ and $G_{qj(r,t)i(m,n)} \triangleq G_{qji} \triangleq G_{q(r,t)(m,n)}$, where $i = i(m,n)$.

Then by (19) and (30) we obtain

$$f_{\emptyset(m,n)}^{(s)} \triangleq f_{\emptyset(m,n)} - f_{\emptyset(m,n)}^{(i)} \;=\; \sum_{r,t} \{k_0^2\ \gamma_\kappa(r,t)\ f_{\emptyset(r,t)}\ g_{(r,t)(m,n)} \;+$$

$$(36)\qquad \gamma_\rho(r,t) \sum_\ell [\delta_{\ell r}^{(1)}\ f_{\emptyset(\ell,t)}\ G_{1(r,t)(m,n)} \;+$$

$$\delta_{\ell t}^{(1)}\ f_{\emptyset(r,\ell)}\ G_{2(r,t)(m,n)}]\}\ .$$

Equation (36) is the complete equation for describing the direct scattering problem with γ_κ and γ_ρ known and the inverse scattering problem with γ_κ and γ_ρ unknown. Note that the sums over r and t are convolutions because of the definitions of the Green's function $g(\underline{x}';\underline{x})$. The sum over ℓ is also a convolution as seen from (20-22). The sums over r,t and ℓ may be rearranged so that all coefficients of each $f_{\emptyset(r,t)}$ are summed and grouped as a total coefficient. Such a form is useful for direct scattering problems where the γ_κ and γ_ρ are

known. This form is given by

$$f^{(s)}_{\emptyset(m,n)} \triangleq f_{\emptyset(m,n)} - f^{(i)}_{\emptyset(m,n)} = \sum_{r,t} \{k_0^2 \gamma_{\kappa(r,t)} g_{(r,t)(m,n)} +$$

(37)

$$\sum_{\ell} [\delta^{(1)}_{r\ell} \gamma_{\rho(\ell,t)} G_{1(\ell,t)(m,n)} + \delta^{(1)}_{t\ell} \gamma_{\rho(r,\ell)} G_{2(r,\ell)(m,n)}]\} f_{\emptyset(r,t)} \quad .$$

We next present methods for obtaining the direct and inverse scattering solutions from (36) and (37) for the special case of $\gamma_\rho(\underline{x}') = 0$. Even with this restriction it will be clear that the general case of $\gamma_\rho(\underline{x}') \neq 0$ may be obtained by extension of the method. This conceptually simple extension requires additional programming complexity and additional memory for storing the coefficients $G_{(r,\ell)(m,n)}$ and is therefore reserved for future publications.

METHODS FOR SOLVING MODEL EQUATIONS FOR CASE OF $\gamma_\rho = 0$

In formulating the direct and inverse scattering solutions for the case $\gamma_\rho = 0$ it will be useful to use the single index notion i to represent a point $\underline{x}_i$ with $i = i(m,n)$, i.e. $\underline{x}_{i(m,n)} = (x_i, y_i) = (mh, nh)$ since the more explicate two index notation (m,n) is now not required. We also emphasize the major role which subscript $\emptyset$ will now play in the inverse scattering solution to obtain unique solutions. In order to obtain a sufficient number of equations to solve for $f^{(s)}_\emptyset$ it will be necessary to also solve for $f_\emptyset(\underline{x})$ inside the body. Thus we must consider two sets of equations, namely, one set relating $f^{(s)}_\emptyset$ anywhere to $f_\emptyset$ inside the body and a second set relating $f_\emptyset$ at point x_i in the body to all other points $\underline{x}_j$ in the body. It will also be useful to write these equations in terms of residuals $r_{1\ell\emptyset}$ and $r_{2m\emptyset}$. Thus we write

$$(38) \qquad r_{1\ell\emptyset} \triangleq f_{\emptyset\ell} - \sum_{j=1}^{N} \gamma_{\kappa j} f_{\emptyset j} C_{\ell j} - f^{(i)}_{\emptyset\ell} = 0 \qquad \begin{matrix} \ell = 1,\ldots,N \\ \emptyset = 1,\ldots,\Phi \end{matrix}$$

$$(39) \qquad r_{2m\phi} \triangleq f_{\phi m}^{(s)} - \sum_{j=1}^{N} \gamma_{\kappa j} f_{\phi j} D_{mj} = 0 \qquad \begin{matrix} m = 1,\ldots,M \\ \phi = 1,\ldots,\Phi \end{matrix}$$

where $c_{\ell j} = k_0^2 g_{j\ell}$ and $D_{mj} = k_0^2 g_{jm}$. The subscript m in (39) refers to a measurement position on a detector. The subscript ℓ in (38) refers to any grid point in a region including the body. By inspection a necessary condition for existance of a common solution to (38) and (39) in that the number of equations exceed the number of unknowns, i.e., that $M\,\Phi \geq N$.

In his study of the direct scattering problem, Richmond [11] obtained a similar set of equations to (38) and (39) above using pulse basis functions. The advantage of the sinc basic functions lies in their economy. Richmond recommends 10 sample points per incident wavelength for his evaluation of $C_{\ell j}$ and D_{mj} to be accurate for problems of low contrast, i.e., $|\gamma_\kappa| \leq .10$. We find that 4 samples per incident wavelength is sufficient for accurate reconstruction of γ_κ for objects whose spatial frequency spectrum of γ_κ does not exceed the reciprocal of the incident wave length. For solving the direct scattering problem, i.e., finding $f_\phi^{(s)}$, we follow the steps in Richmond's method, namely: first, for given γ_κ solve the linear system (38) for $f_{\phi j}$, second, for $f_{\phi j}$ from step one, and for given γ_κ compute $f_{\phi m}^{(s)}$ by evaluating the sum in (39).

Solving the inverse scattering problem is more difficult since both γ_j and $f_{\phi j}$ are unknown and are present in (38) and (39) as quadratic terms or products $\gamma_j f_{\phi j}$. We have investigated [16,17] three methods for solving this nonlinear problem: (1) iteratively solving alternate linear systems method, i.e., solving of (38) for $f_{\phi j}$ with $\gamma_{\kappa j}$ fixed then solving (39) for $\gamma_{\kappa j}$ with $f_{\phi j}$ fixed, (2) nonlinear row action methods [18]. (3) and optimization techniques [19,20]. The last two methods are complex and have not been computationally faster than the first method [17] so we only describe the alternate iterative method (or AIM method for short).

The AIM method for iteratively solving alternate linear systems may be described by the following algorithm: Let $f_{\phi}^{(k)}$ or $\gamma^{(k)}$ be the kth iterate of f_{ϕ} or γ respectively. Then

1. Pick a trial value for $\gamma^{(k)}(\underline{x})$ and $f_{\phi}^{(k)}(\underline{x})$. Pick accuracy δ .
2. Solve (38) for $f_{\phi}^{(k+1)}(\underline{x})$ with $\gamma^{(k)}(x)$ fixed.
3. Solve (39) for $\gamma^{(k+1)}$ with $f_{\phi}^{(k+1)}(\underline{x})$ fixed.
4. Test for convergence by forming the objective function.

$$F_{OBJ} = \sum_{\phi} \sum_{\ell} |r_{1\ell\phi}| + \sum_{\phi} \sum_{m} |r_{2m\phi}| \quad . \tag{40}$$

If $F_{OBJ} < \delta$, go to step 5, else go to step 2.

5. Stop. Print results, make file, display image, etc.

Various methods for solving the linear systems may be employed such as Gauss elimination, fixed point methods (applicable only to equation (38)), e.g.

$$f_{\phi\ell}^{(k+1)} = \sum_{j=1}^{N} \gamma_{kj}^{(k)} f_{\phi j}^{(k)} C_{\ell j} - f_{\phi\ell}^{(i)} \tag{41}$$

or the Kaczmarz method [21,22].

RESULTS OF COMPUTER SIMULATION STUDIES

The performance of the 5-step algorithm for obtaining γ_K for the case $\gamma_\rho = 0$ was investigated using an 11 by 11 pixel test object. Simulated scattering data was obtained by the following two steps: First solve equation (38) for $f_{\phi\ell}$, with γ_{Kj} given by the values of the test object. Second using the $f_{\phi\ell}$ values so obtained and the given γ_{Kj} values, evaluate $f_{\phi m}^{(s)}$ from equation (39). The values of $f_{\phi m}^{(s)}$ thus obtained represent noise free data or $f_{TRUE}^{(s)}$. The distribution is normalized such that $\|\Delta f^{(s)}\|_1 / \|f_{TRUE}^{(s)}\|_1 = \beta$. Here $\|\cdot\|_1$ means the "L one norm" (also called L_1 norm, $\|f\|_1 = \Sigma|f_i|$) . Thus noisy data $f^{(s)} = f_{TRUE}^{(s)} + \Delta f^{(s)}$ is obtained for algorithm evaluation.

Figure 1 shows the 11 by 11 test object. Figures 2-3 show the inverse scattering solution obtained using noisy scattering data with $\beta = .10$, the data over-determined such that $M\Phi = 2.4N$, and the image band limited to have no spatial frequencies higher than the reciprocal of the incident fields wave length. The detector radius was 10 incident field wave lengths and the pixel separation was one fourth incident field wave lengths. If a picture quality index or "one norm error rate" $\alpha = \|\gamma_{picture} - \gamma_{TRUE}\|_1 / \|\gamma_{TRUE}\|_1$ is computed it is seen that $\alpha \approx .06$. Without the spatial filtering $\alpha \approx .17$. These results suggest that with over-determination of the data, with small contrast i.e., $|\gamma| \leq .10$, with a small detector radius, and with a small number of pixels (here $N = 11 \times 11 = 121$) the problem is very well posed.

The question of the effect of increasing the number of pixels N and the contrast in γ on the noise properties of the solution image was investigated. We also investigated the effect of increasing the detector radius. This investigation was conducted to determine the inverse scattering solution when the internal fields were known with certainty. An image computed using the 5-step algorithm, could not have less noise than the a method using the correct internal fields. The solution to the inverse scattering problem with the correct internal fields given, i.e., evaluating (39) for γ, we call the "pseudo inverse scattering problem" [23]. The simultaneous solution of equations (38) and (39) we call the "complete inverse scattering problem" [23].

Our study was composed of the following 6 steps which provide two different upper bounds or estimates on the noise present in the solution to the complete inverse scattering problem.

1. Generate the scattered field data which would be observed at a detector using a Gaussian object distribution. Define $\underline{f}^{(s)}$ as the composite column vector of ΦM components given by

(42a) $$\underline{f}^{(s)} \triangleq \{\underline{f}_1^{(s)}, \underline{f}_2^{(s)}, \ldots, \underline{f}_{\emptyset}^{(s)}, \ldots, \underline{f}_{\Phi}^{(s)}\}^T$$

where

(42b) $$\underline{f}_{\emptyset}^{(s)} \triangleq \{f_{\emptyset}^{(sc)}(\underline{x}_1), \ldots, f_{\emptyset}^{(sc)}(\underline{x}_j), \ldots, f_{\emptyset}^{(sc)}(\underline{x}_M)\} \quad .$$

2. Generate a Gaussian random noise vector $\Delta\underline{f}^{(s)}$ with a mean of zero and normalized such that

(43) $$\frac{\|\Delta\underline{f}^{(s)}\|_1}{\|\underline{f}^{(s)}\|_1} = \beta \quad .$$

3. Starting with the overdetermined linear system (39)

(44) $$A\underline{\gamma} = \underline{f}^{(s)}$$

the least squares solution for $\underline{\gamma}$ which we accept as "the best solution," is obtained by solving:

(45) $$A^H A\underline{\gamma} = A^H\underline{f}^{(s)} \quad .$$

Here A^H is the complex conjugate transpose of A.

4. Compute the "upper bound on the norm error ratio in $\Delta\underline{\gamma}$," B_U, using the condition number inequality [23, page 431].

(46) $$\frac{\|\Delta\underline{\gamma}\|_1}{\|\underline{\gamma}\|_1} \leq K_1(A^H A) \frac{\|A^H\Delta\underline{f}^{(s)}\|_2}{\|A^H\underline{f}^{(s)}\|_1} \triangleq B_U \quad .$$

Here $K_1(A^H A)$ is the one norm condition number of $A^H A$.

5. Determine the actual norm error from the true value of $\gamma(\underline{x}_j)$, i.e., γ_{TRUE} , by solving for $(\gamma_{TRUE} + \Delta\gamma) = \gamma_N$ from the equation

$$A^H A(\gamma_{TRUE} + \Delta\gamma) = A^H(\underline{f}^s + \Delta\underline{f}^s) \quad . \tag{47}$$

6. Determine $\Delta\gamma$ by solving (47) for $(\gamma_{TRUE} + \Delta\gamma)$ and compute the "one norm error ratio of the image" or α by

$$\frac{\|\Delta\gamma\|_1}{\|\gamma_{TRUE}\|_1} \triangleq \alpha \quad . \tag{48}$$

From this type of analysis of the pseudo-inverse problem, we have found the following trends.

1. For a given grid spacing h , the condition number $K_1(A^H A)$ is an exponentially increasing function of the edge dimension $n = N^{1/2}$ of the square imaging grid.
2. Although the condition number and, hence, the error bound in (46) are exponentially increasing with increasing edge dimension, the actual error as computed by (48) does <u>not</u> show this increase with edge dimension.
3. The amount of overdetermination required to make the norm error in the image as low as the norm error in the scattered field is extensive, as much as 300 percent.
4. For weakly overdetermined systems, increasing the detector radius significantly increases the condition number, but for strongly overdetermined systems, it makes very little difference.
5. Increasing the percentage overdetermination improves (decreases) both the upper bound B_U and the actual norm error α in the image.

6. For a fixed radius and number of pixels and for fixed noise in the scattered field, the condition number and noise in the computed image of γ both decrease as the contrast in the test object is increased. For example, for detector radius R = 10 and 300 percent overdetermined data and for a 7 by 7 image, the condition number and noise are 860 and 6 percent, respectively, for a test object consisting of a centered Gaussian radial distribution having a peak complex value γ of 0.1-i 0.01, but the condition number and noise are 200 and 4 percent, respectively, for the same test object with Gaussian peak of 1.0-i 0.1 .

SUMMARY

Presently clinical ultrasound imaging is done almost exclusively with the B-scan mode (a 2-D echo strength to brightness mode) with A-scan (an amplitude of echo graph along a single line) or with Doppler scanning (for measuring blood flow velocity). Ultrasound transmission computed tomography has not found clinical application yet because of the low resolution (no better than 5 to 10 mm) of the time of flight and attenuation images. An improved transmission technique called diffraction tomography is based on perturbation solutions to the Helmholtz wave equation and in principle provide improved resolution for very low attenuating objects, but has as yet not been implemented due to significantly large attenuation in tissues. Diffraction tomography is based on the use of the so called Born or Rytov approximation and therefore does not provide a complete description of wave phenomena.

We have developed a method for solving an exact wave integral wave equation for an inverse scattering solution for both the compressibility and density distributions in a body. Our method depends on the use of multiple incident fields and the representation of the total fields and material properties in a basis function expansion. These techniques are modifications of the moment method or Galerkin method. The solutions obtained by this method, when redundant data are

used, are unique and are stable even with noisy data. We illustrate the robustness of our method by presenting a solution image made with 10 percent noisy data. We also provide tabulated data from experiments which show the effect of picture size (number of pixels) and degree of overdetermination on the image quality. The present algorithms used for obtaining a solution require an enormous amount of computation and therefore are too slow and expensive for clinical applications [24]. Improvements in algorithms speed [24] and anticipated advances in computer technology could open applications for laboratory scanning and eventually perhaps even for clinical scanning for Galerkin or moment method solutions. The demonstration of the accuracy and robustness of these new methods for a small number of pixels should act as an incentive for further research into method of moment or other more exact approaches to inverse scattering.

ACKNOWLEDGMENTS

We acknowledge the work of Michael L. Tracy in writing the FORTRAN programs which provided the images in Figures 1 and 2 and for conducting the study which produced Table 1. A more complete description of this study has been made [17].

Discussion with T. H. Yoon, S. Y. Shin, J. W. Ra, Z. H. Cho, S. B. Park, and G. H. Kim of the Department of Electrical Engineering, Korea Advanced Institute of Science and Technology, Seoul, Korea, are appreciated. Exchanges of information with M. J. Hagmann, now at the National Institutes of Health, Bethesda, Maryland, are also appreciated. We appreciate discussion on iterative methods for solving nonlinear equations with C. Wilcox, Department of Mathematics, University of Utah. The support of our colleagues M. J. Berggren and D. A. Christensen is appreciated. The editing and typing help of Sylvia Morris in the Department of Mathematics, University of Utah is also appreciated. Support in part from grants PDP-110B from the American Cancer Society and R01-CA1-29728 from the National Cancer Institute are appreciated.

REFERENCES

1. Morse, P. M. and K. V. Ingard, *Theoretical Acoustics*, 1968, McGraw-Hill Book Company, New York.

2. Greenleaf, J. F., S. A. Johnson, S. L. Lee, G. T. Herman, and E. H. Wood, *Algebraic Reconstruction of Spatial Distributions of Acoustic Absorption within Tissue from their Two-dimensional Acoustic Projections*, Acoustical Holography, Vol. 5, (Phillip S. Green, editor), Plenum Press, New York, 1974, pp. 591-603.

3. Greenleaf, J. F., S. A. Johnson, W. F. Samayoa, and F. A. Duck, *Algebraic Reconstruction of Spatial Distributions of Acoustic Velocities in Tissue from their Time-of-flight Profiles*, Acoustical Holography, Vol. 6, (Newell Booth, editor), Plenum Press, New York, 1975, pp. 71-90.

4. Wolf, Emil, *Three-dimensional Structure Determination of Semi-Transparent Objects from Holographic Data*, Optics Communicator, Vol. 1, No. 4, 1969, pp. 153-156.

5. Mueller, R. K., M. Kaveh, and G. Wade, *Reconstructive Tomography and Applications to Ultrasonics*, Proceedings of the IEEE, Vol. 67, 1979, p. 567.

6. Kaveh, M., M. Soumekh, Z. Q. Lu, R. K. Mueller, *Further Results on Diffraction Tomography*, Acoustical Imaging, Vol. 12, Plenum Press, 1982, pp. 599-608.

7. Norton, S. J. and M. Linzer, *Correcting for Ray Refraction in Velocity and Attenuation Tomography: A Perturbation Approach*, Ultrasonic Imaging, Vol. 4, 1982, pp. 201-233.

8. Stenger, F., *Asymptotic Ultrasonic Inversion Based on Using More than One Frequency*, Acoustical Imaging, Vol. 11, Plenum Press, 1982, pp. 425-444.

9. Stenger, F., M. J. Berggren, S. A. Johnson, and C. H. Wilcox, *Rational Function Frequency Extrapolation in Ultrasonic Tomography*, submitted to Ultrasonic Imaging in January, 1983.

10. Harrington, R. F., *Field Computation by Moment Methods*, The Macmillan Co., Inc., New York; copies may also be obtained from the author in the Electrical Engineering Department, Syracuse University, Syracuse, New York.

11. Richmond, J., *Scattering by a Dielectric Cylinder of Arbitrary Cross-Sectional Shape*, IEEE Transactions on Antennas and Propagation, May 1965, pp. 334-341.

12. Hagmann, M. J., O. P. Gandhi, and D. K. Ghodgaonkar, *Application of Moment Methods to Electromagnetic Biological Imaging*, MIT's International Microwave Symposium Digest, 1981, p. 432.

13. Yoon, T. H., S. Y. Kim, and J. W. Ra, *Reconstruction of Distributed Dielectric Objects Using Low-Frequency Waves*, Conference Proceedings of the 1982 International GeoScience and Remote Sensing Symposium, Munich, Germany, June 1982; IEEE Transactions on GeoScience and Remote Sensing, IEEE Symposium Digest, Vol. 3, pp. 3.1-4.

14. Johnson, S. A., T. H. Yoon, and J. W. Ra, *Inverse Scattering Solutions of the Scalar Helmholtz Wave Equation by a Multiple Source Moment Method,* Electronics Letters, Vol. 19, No. 4, February, 1983, p. 130.

15. Stenger, F., *Numerical Methods Based on Whittaker Cardinal, or Sinc Functions,* SIAM Review, Vol. 23, No. 2, April, 1981.

16. Johnson, S. A., M. L. Tracy, *Inverse Scattering Solutions by a Sinc Basic, Multiple Source, Moment Method-Part I: Theory,* submitted to Acoustical Imaging.

17. Tracy, M. L., and S. A. Johnson, *Inverse Scattering Solutions by a Sinc Basic, Multiple Source, Moment Method-Part II: Numerical Evaluations,* submitted to Acoustical Imaging, May, 1983.

18. Censor, Y., *Raw-Action Methods for Huge and Sparce Systems and Their Applications,* SIAM Review, Vol. 23, No. 4, October, 1981, pp. 446-466.

19. Fletcher, R., *Practical Methods of Optimization, Vol. 1, Unconstrained Optimization,* John Wiley & Sons, New York, 1980.

20. Gill, P. E., W. Murray, M. H. Wright, *Practical Optimization,* Academic Press, 1981.

21. Kaczmarz, S., *Angenaherte Auflosung von System Linearer Gleichungen,* Bull. Akad. Polon. Science Lett., A. 35, 1935, pp. 355-357.

22. Herman, G. T., *Image Reconstruction from Projections, The Fundamentals of Computerized Tomography,* Academic Press, New York, 1980.

23. Ralson, A., and P. Rabinowitz, *A First Course in Numerical Analysis,* McGraw-Hill Book Company, New York, 1978.

24. Fast imaging algorithms based upon Fast Fourier Transform (FFT) implementation of the back projection algorithm

$$\gamma_\ell \approx \mathrm{FFT}^{-1}\{\mathrm{FFT}[\gamma'_\ell]/\mathrm{FFT}[\mathrm{sinc}(k_0|\underline{x}|)]\}$$

where

$$\sum_i^N \gamma_\ell \,\mathrm{sinc}(k_0|\underline{x}_\ell - \underline{x}_i|) \approx \gamma'_\ell = \frac{2\pi}{\Phi}\sum_\phi^\Phi (1/f_{\phi\ell}) \sum_m^M f_{\phi m} D^*_{m\ell}$$

for solving Equation (39) and Fast Fourier Transform implementation of conjugate gradient methods for solving Equation (38) look promising for reducing computational time dependence from $N^{5/2}$ of this paper to $N^{3/2} \log N$. These suggestions were made by S. A. Johnson and D. T. Borup, respectively, Department of Electrical Engineering, University of Utah, prior to April 1, 1983.

$r = 10\ \lambda$ $\gamma < 0.1 - j0.01$ 5% Noise	50% Over		100% Over		200% Over		300% Over	
	B_U	α	B_U	α	B_U	α	B_U	α
3 x 3	---	---	45.0	.70	.27	.083	.22	.093
5 x 5	220	.91	8.7	.12	.74	.057	.84	.049
7 x 7	4×10^4	4.90	220.0	.47	15.00	.140	6.40	.060

TABLE 1. Upper bound on the norm error B_U and actual norm error α for various size images as function of percent overdetermination of the problem. Constant grid spacing $h = 1/4\ \lambda$, problem size is N×N, detector radius is at 10 wavelengths. Five percent Gaussian noise was added to the scattered field. A two-dimensional Gaussian test object similar to that in Figure 1 was used.

0	0	1	4	8	10	8	4	1	0	0
0	0	0	0	0	-1	0	0	0	0	0
0	2	10	25	43	52	43	25	10	2	0
0	0	-1	-2	-1	-5	-1	-2	-1	0	0
1	10	36	91	158	190	158	91	36	10	1
0	-1	-3	-9	-15	-19	-15	-9	-3	-1	0
4	25	91	229	398	478	398	229	91	25	4
0	-2	-9	-22	-39	-47	-39	-22	-9	-2	0
8	43	158	398	691	831	691	398	158	43	8
0	-1	-15	-39	-69	-83	-69	-39	-15	-4	0
10	52	190	478	831	1000	831	478	190	52	10
-1	-5	-19	-47	-83	-100	-83	-47	-19	-5	-1
8	43	158	398	691	831	691	398	158	43	8
0	-4	-15	-39	-69	-83	-69	-39	-15	-4	0
4	25	91	229	398	478	398	229	91	25	4
0	-2	-9	-22	-39	-47	-39	-22	-9	-2	0
1	10	36	91	158	190	158	91	36	10	1
0	-1	-3	-9	-15	-19	-15	-9	-3	-1	0
0	2	10	25	43	52	43	25	10	2	0
0	0	-1	-2	-4	-5	-4	-2	-1	0	0
0	0	1	4	8	10	8	4	1	0	0
0	0	0	0	0	-1	0	0	0	0	0

FIGURE 1. An 11 by 11 image of a Gaussian test object. The pixels, i.e., grid points, are separated by 1/4 wavelength. Thus, the image is 11/4 by 11/4 wavelengths. Each pair of upper and lower numbers corresponds to a scaled value of γ_k at each grid point. The top number in each pair is 10,000 times the value of the real part of γ_k and the bottom number is 10,000 times the imaginary part of γ_k. Using this test object, simulated scattering data was obtained using the method of moments to solve the direct solution. Ten percent Gaussian random noise was then added to the simulated scattering data, i.e., the ratio of the one norm of the noise to the one norm of the scattering data is ten percent. The simulated scattering data with noise thus generated was used as input for the method of moments inverse scattering solution method. The results of the calculations to retrive the original object are shown in the next figure.

16	6	-2	-2	20	8	-9	2	20	-29	38
12	0	-14	-2	-35	43	-22	19	-2	-14	-21
-3	33	-17	29	40	68	69	12	-3	49	-27
-8	12	-6	-10	45	-33	42	-30	0	5	-10
3	-18	52	91	164	205	118	100	21	-19	21
30	-15	7	-14	-49	1	-71	22	0	-2	14
3	38	85	215	377	454	458	200	97	26	-4
-12	30	-16	-25	-65	-51	-20	-34	-13	14	-14
-8	37	186	365	706	830	635	403	186	48	10
19	-39	-4	-80	-61	-81	-60	-24	7	-46	13
18	39	204	479	834	1004	839	485	192	54	-5
-5	21	-43	-37	-90	-86	-72	-34	-34	-13	-25
-2	34	157	411	695	825	704	383	163	28	-5
-21	26	-30	-43	-71	-98	-91	-18	-14	-25	0
8	24	131	225	373	495	393	234	68	61	18
14	-42	3	-34	-33	-52	-25	-29	5	12	0
11	5	34	72	162	191	179	79	37	-13	-22
-8	46	-40	9	-25	-23	4	1	16	-38	28
-18	12	26	-11	74	47	41	16	23	9	15
-9	-18	41	-13	-2	6	-11	-3	-31	27	-31
14	9	-2	13	15	22	-1	20	5	24	-4
-20	15	-25	38	-11	16	-12	16	24	0	23

FIGURE 2. Reconstructed image of object shown in Figure 1 using the method of moments without spatial filtering. The image was made from simulated scattered data with ten percent added noise using the test object of Figure 1 and the iterative reconstruction algorithm described in the text. The above results after 20 iterations shows about 17 percent noise, i.e., $\alpha = 0.17$ from equation (48).

0	-2	0	8	17	18	11	3	2	5	6
2	0	-4	-3	1	6	6	1	-4	-8	-8
1	0	4	20	41	49	37	15	2	2	5
4	1	-2	-4	-3	-2	-2	-2	-1	-1	-2
3	8	31	86	153	186	157	87	27	3	3
6	4	-3	-15	-22	-23	-17	-8	0	4	3
5	21	89	234	400	477	406	240	90	18	4
6	4	-11	-36	-53	-52	-36	-18	-7	-2	0
7	33	156	409	688	811	688	412	162	38	8
2	0	-20	-53	-80	-80	-57	-31	-17	-14	-9
8	39	188	491	823	967	817	488	192	45	10
-1	-4	-23	-56	-88	-93	-70	-39	-21	-17	-13
8	36	161	416	698	822	695	410	155	32	8
-1	-4	-18	-45	-73	-82	-64	-34	-14	-9	-8
7	25	95	241	408	487	414	240	83	13	4
0	0	-9	-27	-45	-51	-39	-19	-5	0	0
6	13	35	86	152	187	160	91	30	4	3
0	1	0	-9	-17	-18	-11	-3	0	1	2
4	4	6	18	36	44	37	22	11	7	4
-3	0	4	3	0	0	2	3	2	0	0
3	1	2	9	17	17	12	9	10	10	4
-5	-2	4	7	5	1	0	2	3	2	0

FIGURE 3. Reconstruction of image shown in Figure 1 using the method of moments and spatial filtering. This image is the spatial filtered version of Figure 2. Since Figure 2 is sampled at 4 samples per wavelength of the incident field the image contains noise frequencies up to twice the reciprocal of the incident fields wave length. Let λ_0 be the incident field's wavelength. Then spatial frequencies in the range from $1/\lambda_0$ to $2/\lambda_0$ may be removed from Figure 2 without effecting the practical resolution limit of the image of γ_k. Figure 3 is the image in Figure 2 filtered in this manner. The noise is reduced considerably since α as defined by equation (48) is reduced from 0.17 in Figure 2 to 0.05 here.

REPORT DOCUMENTATION PAGE

READ INSTRUCTIONS BEFORE COMPLETING FORM

1. REPORT NUMBER	2. GOVT ACCESSION NO. AD-A131 408 / 3. RECIPIENT'S CATALOG NUMBER
4. TITLE (and Subtitle) ULTRASOUND TOMOGRAPHY BY GALERKIN OR MOMENT METHODS	5. TYPE OF REPORT & PERIOD COVERED
	6. PERFORMING ORG. REPORT NUMBER
7. AUTHOR(s) Frank Stenger and Steven A Johnson	8. CONTRACT OR GRANT NUMBER(s) DAAG-29-83-K-0012
9. PERFORMING ORGANIZATION NAME AND ADDRESS University of Utah, Department of Mathematics Salt Lake City, UT 84112	10. PROGRAM ELEMENT, PROJECT, TASK AREA & WORK UNIT NUMBERS
11. CONTROLLING OFFICE NAME AND ADDRESS	12. REPORT DATE May 5, 1983
	13. NUMBER OF PAGES 28
14. MONITORING AGENCY NAME & ADDRESS(if different from Controlling Office)	15. SECURITY CLASS. (of this report) UNCLASSIFIED
	15a. DECLASSIFICATION/DOWNGRADING SCHEDULE

16. DISTRIBUTION STATEMENT (of this Report)

Approved for public release, distribution unlimited

17. DISTRIBUTION STATEMENT (of the abstract entered in Block 20, if different from Report)

18. SUPPLEMENTARY NOTES

The findings of this report are not to be construed as an official Department of the Army position, unless so designated by other authorized documents.

19. KEY WORDS (Continue on reverse side if necessary and identify by block number)

20. ABSTRACT (Continue on reverse side if necessary and identify by block number)

SEE ATTACHED PAGE

DD FORM 1 JAN 73 1473

ABSTRACT

This paper describes a Galerkin scheme which uses a sinc basis (i.e., translations of $\sin(\pi x)/(\pi x)$ --[15]) to carry out an ultrasonic tomography inversion based on the equation

$$(1) \qquad \nabla^2 f + k^2 f = -k^2 \gamma_\kappa f - \nabla\cdot[\gamma_\rho \nabla f] \ .$$

In (1), f denotes the sound pressure, $k = 2\pi \times \text{frequency} \times \sqrt{\kappa_0 \rho_0}$, $\gamma_\kappa = (\kappa-\kappa_0)/\kappa_0$, $\gamma_\rho = (\rho-\rho_0)/\rho_0$ where κ (rsp. κ_0) denotes the compressibility of the body (rsp. the fluid surrounding the body) and ρ (rsp. ρ_0) denotes the corresponding density. The reconstruction of the functions γ_κ and γ_ρ in $\mathbb{R}^2$ (n = 2 or 3) is based on measuring the sound pressure f on a finite number of n-1 dimensional hyperplanes for each fixed source, and then repeating the experiment using a finite number of source positions. The process is nonlinear, since all of f , γ_ρ and γ_κ must be reconstructed in the interior of the body. We thus describe an iterative procedure for carrying out the reconstruction. An example is described, illustrating a two dimensional reconstruction in the presence of 10% Gaussian noise.

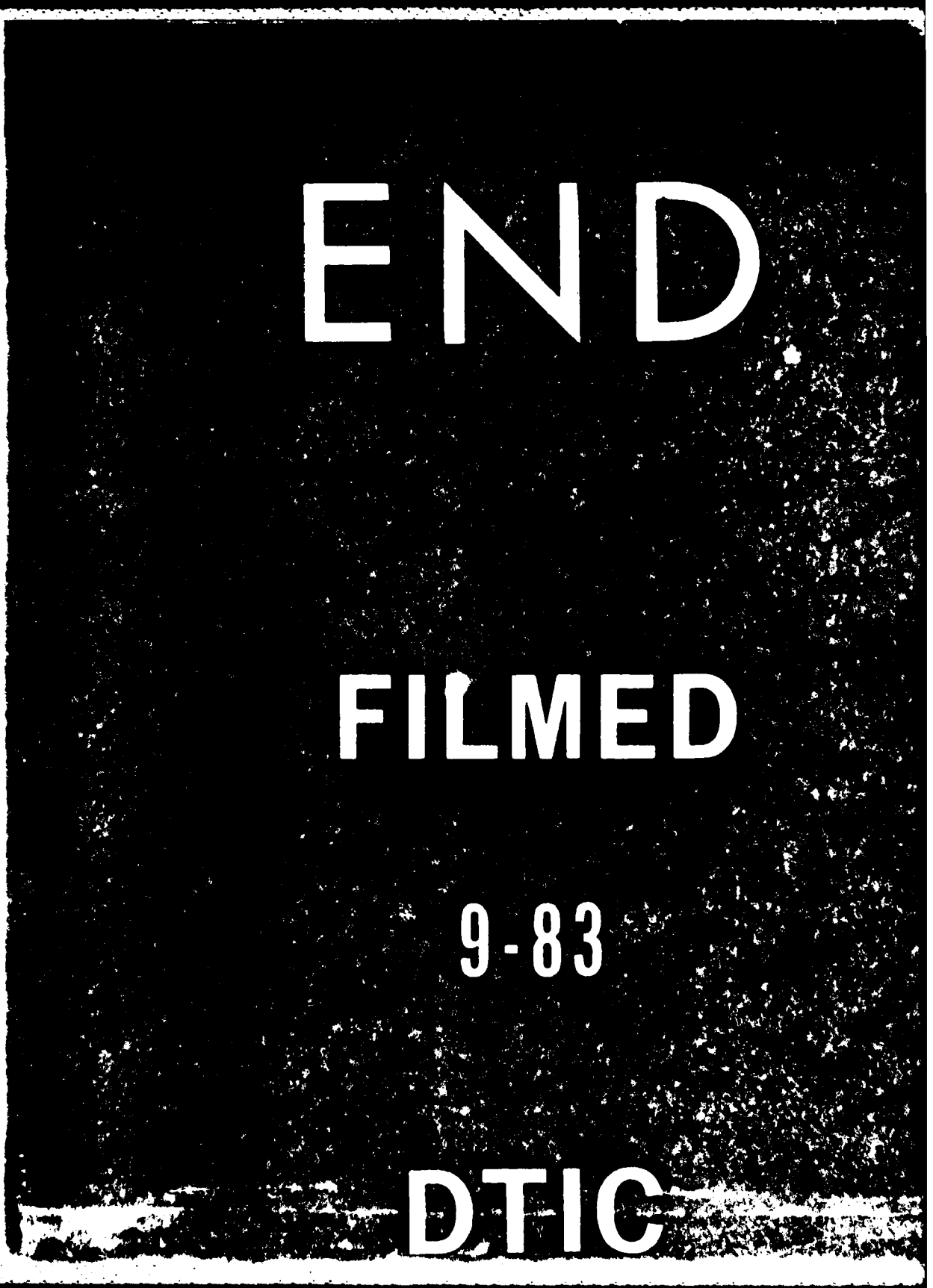
END
FILMED
9-83
DTIC